Available at www.sciencedirect.com

ScienceDirect

journal homepage: www.elsevier.com/locate/watres

Coagulation behavior of Al_{13} aggregates

Jr-Lin Lin[a], *Ching-Ju M. Chin*[b], *Chihpin Huang*[a,*], *Jill R. Pan*[c], *Dongsheng Wang*[d]

[a]*Institute of Environmental Engineering, National Chiao-Tung University, 75 Po-Ai Street, Hsinchu, Taiwan*
[b]*Institute of Environmental Engineering, National Central University, Jungli, Taiwan*
[c]*Department of Biological Science and Technology, National Chiao-Tung, University, Taichung, Taiwan*
[d]*SKLEAC, Res. Center for Eco-Envir. Sci., Chinese Academy of Sciences, Beijing, China*

ARTICLE INFO

Article history:
Received 10 March 2008
Received in revised form
8 July 2008
Accepted 10 July 2008
Available online 31 July 2008

Keywords:
PACl
Coagulation
Al_{13} aggregates
Kaolin
Fractal dimension

ABSTRACT

The coagulation behavior of Al_{13} aggregates formed in coagulation of kaolin was investigated by small angle static light scattering (SASLS), solid-state ^{27}Al NMR and tapping mode atomic force microscope (TM-AFM). A kaolin suspension was coagulated by PACl containing high content of Al_{13} polycation (PACl-Al_{13}). The results indicated that Al_{13} was predominant in destabilizing kaolin particles for PACl-Al_{13} coagulation even though at alkaline pH (pH 10). At such high pH, Al_{13} aggregates were observed when the dosage of PACl-Al_{13} was increased. In addition, the mechanism of coagulation by PACl-Al_{13} at alkaline pH was affected by dosage. When the dosage was insufficient, coagulation was caused by electrostatic patch, which led to compact flocs with high fractal dimension (D_f). Interparticle bridging dominated the coagulation when the coagulant dosage approached the plateau of adsorption, which caused the looser flocs with low D_f. The in-situ AFM scanning in liquid system proved that the existence of linear Al_{13} aggregates composed of a chain of coiled Al_{13} in coagulation by PACl-Al_{13} at a high dosage and alkaline pH. Meanwhile, several coiled Al_{13} aggregates with various dimensions were observed at such condition.

1. Introduction

Polyaluminum chloride (PACl) has been commonly applied to remove colloidal particles and organic matters in water and wastewater treatments. Effective coagulation by PACl depends on the interaction between the aluminum hydrolysis species and particles as well as organic matters. The hydrolysis products of PACl comprise a series of Al species contributing different mechanisms and efficiencies in coagulation. Many studies have proven that the Al(III) species can transform into polymers by controlling the $[OH^-]/[Al]$ ratio during the preparation of PACl (Akitt and Farthing, 1981; Bottero et al., 1980; Liu et al., 1999). The most well-known polymer of Al is Al_{13} polycation, $[AlO_4Al_{12}(OH)_{24}(H_2O)_{12}]^{7+}$, which is composed of a $Al(O)_4$ tetrahedron surrounded by 12 octahedrally coordinated Al sharing edges (i.e. ϵ-Keggin structure) (Johansson, 1960), has been commonly accepted as the critical species in particle aggregation by strong charge neutralization (Lin et al., 2008; Wang and Hsu, 1994).

Al_{13} is metastable with respect to $Al(OH)_3$ and transforms to various $Al(OH)_3$ such as gibbsite and bayerite over time upon the hydrolysis processes (Violante and Huang, 1985; Bradley et al., 1993). The condensation of Al_{13} could form at a specific pH due to shear-induced mixing (Furrer et al., 2002). During condensation, Al_{13} can transform into various Al_{13} aggregates with increasing [OH]/[Al] ratio and total Al concentration (Bottero et al., 1987). Al_{13} aggregates can be decomposed by H^+ as the pH value decreases (Furrer et al., 1992). Furthermore, different oxygen sites of Al_{13} have different water exchange rates which relate to

* *Corresponding author*. Tel.: +886 3 5726463; fax: +886 3 5725958.
E-mail address: cphuang@mail.nctu.edu.tw (C. Huang).
0043-1354/$ – see front matter
doi:10.1016/j.watres.2008.07.028

decomposition of Al_{13} (Phillips et al., 2000). However, there are debates on the formation pathway of the Al_{13} aggregates, which depends on the reaction conditions such as Al concentration, pH, temperature, and aging processes (Sposito, 1996). For coagulation of natural waters, pH value affects coagulation mechanisms significantly, especially for low pH. Generally, the coagulation mechanisms induced by aluminum salts favor charge neutralization at quite low aluminum concentrations and low pH (Letterman et al., 1982). If the positively charged species are adsorbed onto the isolated regions of particles, then the ''electrostatic patch'' attraction may be important as in the case of polyelectrolytes (Gregory, 1973). Dentel (1988) also has proposed the precipitation charge neutralization (PCN) to explain that charge neutralization can be achieved by partial coverage of positively charged hydroxide on negatively charged particle surface.

Recently, many researchers have well clarified that the coagulation behavior of Al_{13} in PACl coagulation of colloids or organic matter (Gao et al., 2005; Hu et al., 2006; Kazpard et al., 2006; Yan et al., 2007). Furthermore, several researches have inferred that Al_{13} aggregates could destabilize particles by either electrostatic patch or bridging when sufficient dosage of PACl is applied or when alkalinity is increased (Chen et al., 2006; Ye et al., 2007; Wu et al., 2007). However, these assumptions have never been verified and could not accurately illustrate the coagulation behavior of Al_{13} aggregates because it is a formidable task to quantify the Al_{13} aggregates. The formation of Al_{13} aggregates during coagulation also has never been observed in-situ and further investigations are necessary to identify the interactions between Al_{13} aggregates and the colloidal particles.

The goal of this study is to investigate the role of Al_{13} aggregates on coagulation via in-situ diagnostic technology. A laboratory prepared coagulant with relatively high content of Al_{13} was dosed in a kaolin suspension. The sizes of aggregates at various dosages were monitored by a small angle static light scattering (SASLS) apparatus. The configuration and morphology of the Al_{13} aggregates were also observed by tapping mode atomic force microscope (TM-AFM) in liquid system.

2. Material and methods

2.1. Kaolin suspension

The purified kaolin (Sigma Chemical Co., USA) was dispersed by RO water for 30 min to a concentration of 2.5 g/L. After 24 h of settling, the supernatant was used as the synthetic stock solution, which was diluted by the RO water to prepare the turbid water samples to the desired turbidity of 50 NTU, which is about 20.3 mg/L. Particle size distribution of the synthetic suspension was analyzed by a particle size analyzer (Master 2000, Malvern Inc., UK). The mean particle size of the synthetic water sample was 2.9 μm. The specific conductivity of the working suspension was adjusted by 10^{-3} M $NaClO_4$ solution (Merck, Inc., USA) and the alkalinity was adjusted by 10^{-3} M Na_2CO_3 (Merck, Inc., USA).

2.2. Characterization of PACl

A PACl product of high Al_{13} content was separated from preformed PACl by sulfate precipitation and nitrate metathesis (Shi et al., 2007). This PACl was named PACl-Al_{13} here. The working solutions containing 1000 mg-Al/L were freshly prepared from the stock solution before each trial. The aluminum concentration was determined by an inductively coupled plasma atomic emission spectrometry (ICP-AES, JY24, Jobin-Yvon Inc., France). The distributions of hydrolyzed Al species of PACl-Al_{13} in solution were determined with a 500 MHz ^{27}Al nuclear magnetic resonance (NMR) (Unityinova-500, Varian, USA). The operation parameters for the NMR analysis were spectrometer frequency, solvent, and temperature, which were 130.24 MHz, D_2O, and 298 K, respectively. A 5-mm sample tube (Wilmad 507-pp, SP Industries Inc., USA) containing 3 mL Al solution and a 4.2-mm sample tube (Wilmad WGS-5BL, SP Industries Inc., USA) containing 1 mL 0.05 M $Al(OD)_4^-$ solution were co-inserted as the inner standard. The chemical shift of $Al(OD)_4^-$ was at 80 ppm. The signals in the proximity of 0 and around 62.5 ppm represent monomeric Al (Al_m) and tridecamer Al_{13}, respectively. The concentration of each species was determined by the ratio of the integrated intensity of the corresponding peak to that of $Al(OD)_4^-$ at 80 ppm. The amount of the undetectable species (denoted as Al_u) was obtained by subtracting the sum of the detected Al species from the total Al concentration. The Al speciation of PACl-Al_{13} is summarized in Table 1. The PACl-Al_{13} contained around 96% Al_{13} with a little amount of Al_u.

2.3. Coagulation experiments

Standard jar tests were conducted in 1-liter beakers to evaluate coagulation efficiencies. The initial rapid mixing was conducted at 200 rpm ($G = 350\ s^{-1}$) for 1 min followed by a slow mixing at 30 rpm ($G = 25\ s^{-1}$) for 20 min. The suspension was left undisturbed for 20 min. After the settling, the residual turbidity (RT) of the supernatant was measured. The zeta potentials (ZP) of the suspension were measured via a laser zeta analyzer (Zetasizer nano ZS, Malvern Inc., UK) immediately after the rapid mixing. All coagulant dosages used in this study were in the unit of mg/L as Al.

To study the effects of dosage on the size of Al_{13} aggregates, the solution without particles were employed as the blank sample. The PACl-Al_{13} was used as a coagulant to evaluate the formation of Al_{13} aggregates after dosing in the blank sample. After the addition of PACl-Al_{13}, the sample was first stirred at 200 rpm for 1 min under pH 10 and then a small amount of sample was withdrawn for size measurement and AFM imaging.

Table 1 – Characterization of PACl-Al_{13} by ^{27}Al NMR method

pH	(%)		
	Al_m	Al_{13}	Al_u
4.7	0	95.8	4.2

2.4. Characterization of aggregates

2.4.1. Size

A particle size analyzer (Mastersizer 2000, Malvern Inc., UK) with a small angle static light scattering (SASLS) was used to directly monitor the dynamics of aggregate growth during coagulation and the structure of kaolin particle aggregates. The similar jar tests were performed to observe the kinetics of coagulation for the study. During coagulation, the suspension was pumped to the SASLS by a peristaltic pump (EW-7553-70, Cole-Parmer Instrument Co., USA) with a Tygon tubing (Masterflex-06409-16, Cole-Parmer Instrument Co., USA) of I.D. 3.1 mm, and the sample was recycled back to the mixing vessel at a flow rate of 20 ml/min. The shear and disruption of aggregates in such setup are negligible.

2.4.2. Structure

A mass fractal is a mathematical description of irregular geometric shapes (Mandelbrot, 1983), which is further applied to demonstrate the complex structure of particle aggregates generated in water and wastewater treatment processes (Guan et al., 1998; Li and Ganczarczyk, 1989). The mass fractal suggests that the structure of an aggregate is self-similar at various length scales or scale invariance. For a mass fractal aggregate, the mass, M, of a fractal with fractal dimension, D_f, is proportional to its size, R, raised to power D_f (Mandelbrot, 1983):

$$M(R) \propto R^{D_f} \tag{1}$$

Static light scattering has been extensively employed to evaluate the size and structure of aggregates as well as in the study of coagulation of various suspensions such as kaolin, latex, and aluminum suspension (Berka and Rice, 2005; Waite et al., 2001). The scattered light intensity I is measured as a function of the magnitude of the scattering vector, Q. The relationship between the scattered intensity from the aggregate, $I(Q)$, and the scattering wave vector, Q, is shown as follow (Lin et al., 1989):

$$I(Q) \propto Q^{-D_f} \tag{2}$$

where

$$Q = \frac{4\pi n \sin(\theta/2)}{\lambda} \tag{3}$$

here, n is the refractive index of the fluid, λ is the wavelength in the vacuum of the static light used, and θ is the scattering angle. The mass fractal dimension D_f can be estimated from the absolute slope of log $I(Q)$ versus log Q by fitting a straight line through the fractal regime section of the scattering plot. This relationship is valid in power low regime where length scales are much larger than the primary particles and much smaller than aggregates. The scattering exponents obtained from SASLS (i.e. D_s) does relate to the structure properties of primary flocs rather than entire flocs, which can be explained by the existence of two-level floc structural model that is derived by other investigators (Wu et al., 2002). In this study, the SASLS experiments have been restricted to the 10^{-3}–4.5×10^{-4} nm^{-1} Q range to allow the power law regime for the structural analysis of primary flocs.

2.4.3. Morphology of Al_{13} aggregates

A Nanoscope III atomic force microscope (Multimode, Digital Instruments Inc.) was used to observe the morphology of Al_{13} aggregates. A ultrasharp silicon cantilever (NSC15, MilkroMasch, Spain), whose spring constant, resonance frequency, and nominal tip radius are 20–75 N/m, 265–400 kHz, and less than 10 nm, respectively, was employed to scan the image of sample in tapping mode atomic force microscope (TM-AFM) that can avoid destruction of samples. TM-AFM has been widely applied in liquid environment to in-situ observe the surface morphology of polymer materials or biological matters, which can prevent the condensation of hydrous samples (Arita et al., 2004; Ikai, 1996). All the experiments here were conducted at room temperature in liquid system.

Before each AFM imaging, mica plates were cleaned by the following process. First, the mica plates were immersed overnight in a 1 M HCl solution. They were then soaked in acetone for 30 min and boiled in a mixture of $5H_2O$:$1H_2O_2$:$1NH_4OH$ at 80°C for 25 min. After that, the mica plates were washed by DI water. The same cleaning process has been used by other studies (Chin et al., 2002; Nalaskowski et al., 1999). Such a cleaned surface is fully wettable by water, and no contamination is detected by AFM.

After the mica plate was cleaned, a drop of Al_{13} solution sample was sampled from the reactor and then dropped onto the mica plates, fixed by adsorption, and immediately measured by TM-AFM. To maintain the AFM imaging in liquids, the mica plate with Al_{13} adsorbed on it was left without resupplying water for at least 1 h and the AFM imaging was conducted until the surface of DI water lowered to the surface of the mica.

2.5. Solid-state ^{27}Al magic-angle spinning nuclear magnetic resonance

The solid-state magic-angle spinning nuclear magnetic resonance (MAS-NMR) spectra were recorded by a Bruker instrument (DSX-400WB, Bruker, Germany) in 4 mm rotors, and the ^{27}Al spectra were recorded at 104.1 MHz. The solid-state ^{27}Al MAS-MNR was performed on freeze-drying PACl-Al_{13} aggregate samples at various dosages. The PACl-Al_{13} aggregates formed after coagulation were immediately freeze dried over 24 h with a vacuum refrigerating instrument (FD2-D, Kingmech Co., Ltd, Taiwan) to separate them from the solution.

2.6. Wet scanning electron microscope (WSEM)

Aggregates formed by PACl-Al_{13} coagulation were withdrawn into a sealed specimen capsule (QX-102, Quantomix Co. Ltd, Israel) and were protected from vacuum in the microscope by an electron-transparent partition membrane. Imaging by this way can make the micron-scale observation of fully hydrated samples or water solution maintained at atmospheric pressure. The detailed descriptions of the specimen capsule were presented elsewhere (Katz et al., 2007). After the placement of samples, the morphology of the wet aggregates was observed by a conventional scanning electron microscope (SEM) (5136LS, Tescan, Czech).

3. Results and discussion

3.1. pH effects on PACl-Al_{13} coagulation

The changes of ZP and RT during coagulation with PACl-Al_{13} are presented in Fig. 1. The dosage of coagulant is 1 mg/L for all conditions in this figure. The efficient turbidity removal of PACl-Al_{13} coagulation occurs in the alkaline pH region. Because the amount of Al_{13} remains stable in the entire pH range (Hu et al., 2006; Wang et al., 2004), the highly positively charged Al_{13} is the major reactive species in the coagulation by PACl-Al_{13}. The maximum turbidity removal occurs at pH 9, where the ZP is somewhat below zero. However, the relatively efficient destabilization of particles with rather negative ZP (−16.7 mV) is also observed at high alkaline pH (pH 10). This indicates that not only charge neutralization is responsible for the particle coagulation in the study. The results could be explained by the effect of the Al_{13} aggregates on particle destabilization.

The size and the electrophoretic mobility of Al_{13} aggregates vary with the solution pH. It has been proven that Al_{13} can aggregate above pH 6 and precipitates form at alkaline conditions (Dubbin and Sposito, 2005; Furrer et al., 1992; Furrer et al., 1999). Al_{13}, which possesses a +7 valence, could be decomposed by deprotonation reactions that release the protons in pairs to yield the Al_{13} with less positive charges such as Al_{13}^{5+} Al_{13}^{3+} and Al_{13}^{+} when the pH was raised (Furrer et al., 1992). As a result, the Al_{13} aggregates can be more easily generated during PACl-Al_{13} coagulation at high pH, and the size of them increases with increasing pH values. Although Rakotonarivo et al. (1988) have addressed that Al_{13} aggregates formed at various Al concentrations almost have zero surface charge at pH 8, other study has indicated that Al_{13} aggregates still result in efficient coagulation at alkaline pH (Chen et al., 2006). As shown in Fig. 2, the aggregates formed at pH 10 are larger in size and lower in D_f, where the ZP is more negative than that at pH 9. The results imply that either electrostatic patch or interparticle bridging may play a more important part in particle coagulation when the Al_{13} aggregates form.

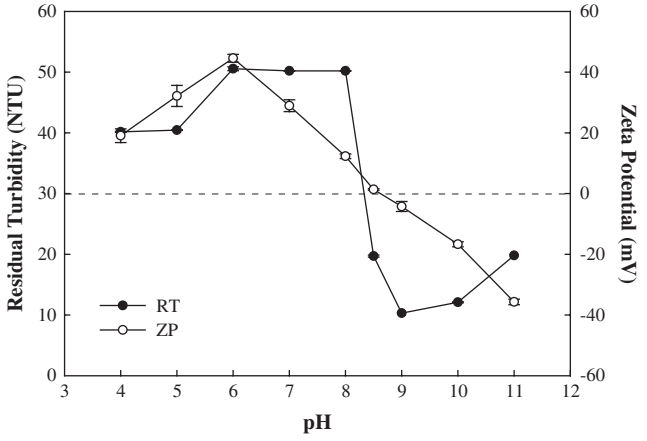

Fig. 1 – The residual turbidity and zeta potential for the PACl-Al_{13} coagulation under various pH values at 1 m/L as Al.

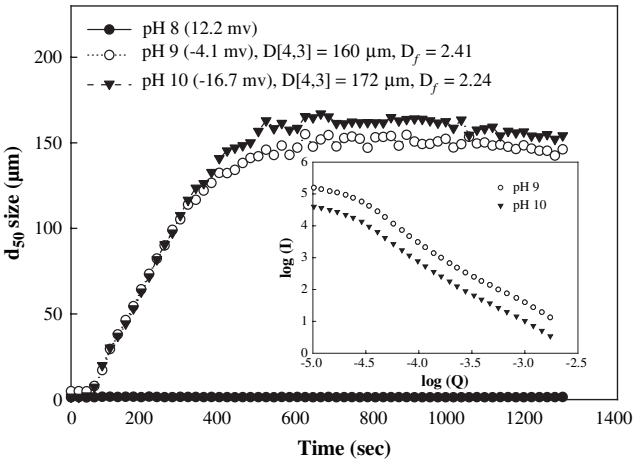

Fig. 2 – Aggregates characteristics of PACl-Al_{13} coagulation at alkaline pH.

3.2. Particle destabilization by Al_{13} aggregates

The occurrence of electrostatic patch or interparticle bridging depends on the dosage for polymer coagulation (Zhou and Franks, 2006). The dosage of PACl-Al_{13} coagulation also influences the amount of hydrolyzed Al species adsorbed onto the surface of particles and the conformation of hydrolyzed polymeric Al species adhered to the surface of the particles, which substantially affects the coagulation mechanism. In order to understand the effects of PACl-Al_{13} dosage on the formation of aggregates during coagulation and how they react with kaolin particles, the PACl-Al_{13} coagulation was conducted at pH 10 where the Al_{13} aggregates are easily formed. The changes in the RT and ZP for PACl-Al_{13} coagulation at various dosages are demonstrated in Fig. 3. The turbidity decreases rapidly after the addition of PACl-Al_{13}, and then reaches a minimum. The magnitude of the negative ZP decreases sharply with increasing dosage when the dosage is lower than 2 mg/L. The ZP levels off and approaches to zero when the dosage is higher than 8 mg/L where the coagulant dosage reaches the plateau of adsorption. Wu et al. (2007) have

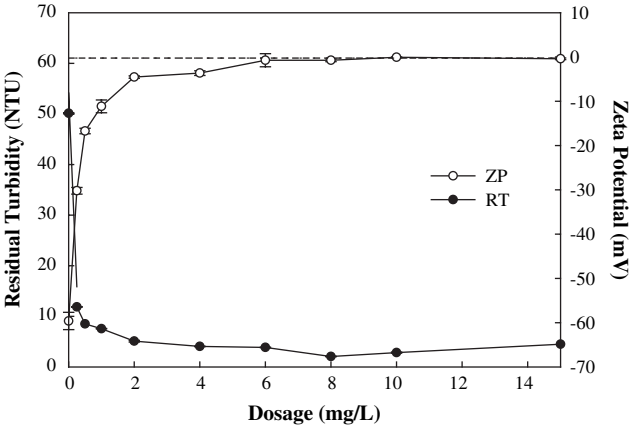

Fig. 3 – The residual turbidity and zeta potential for PACl-Al_{13} coagulation at pH 10 under various dosages.

indicated that highly positively charged Al_{13} adsorbs onto the surface of particles by monolayer adsorption. Then, the saturation of surface coverage occurs rapidly and the restabilization of particles is found due to the strong repulsion between polycations. However, the destabilized particles with zero ZP at high dosage are still found in our study, which could be interpreted by the low charge neutralization ability of Al_{13} aggregates at pH 10.

Because Al_{13} with less positive charges occurs at alkaline pH, the repulsions between Al_{13} become weaker, which facilitate the self-aggregation of Al_{13}. Also, the Al_{13} deprotonation also varies with the concentration of the Al_{13} (Furrer et al., 1992). The Al_{13} becomes more acidic at higher concentrations, and the aggregation of Al_{13} at higher concentrations promotes the release of H^+; as the consequence, the charge of Al_{13} is less positive. On the other hand, the Al_{13} aggregates could not rapidly form at low dosage during PACl-Al_{13} coagulation at alkaline pH because Al_{13} does not easily aggregate before reacting with kaolin particles, which influences the charge of Al_{13} and its adsorption on the surface of particles. Thus, at alkaline pH the distinct different coagulation mechanisms could be performed in the PACl-Al_{13} coagulation at low and high dosages.

To verify that whether the Al_{13} would transform into other species such as gibbsite or bayerite, the solid-state ^{27}Al NMR was used to identify the Al speciation within the aggregates. Fig. 4 shows the solid-state ^{27}Al NMR spectra of the aggregates coagulated with PACl-Al_{13} at pH 10 with low and high dosages, respectively. The spectra for the aggregates formed at 8 mg/L exhibited two distinctive resonances at about 0 ppm and 63 ppm, while the spectra for the aggregates coagulated with PACl-Al_{13} at 1 mg/L displayed one prominent resonance at 0 ppm and very weak resonance at 63 ppm.

The symmetric peak at 0 ppm corresponds to octahedrally coordinated aluminum and the peak at 63 ppm corresponds to tetrahedral aluminum (Bertsch et al., 1986b; Bottero et al., 1980). An intensive peak at 0 ppm was obtained in all cases due to the existence of octahedral aluminum structure in the kaolin particles (Sanz and Serratosa, 1984). Because of the weaker surface charge of the Al_{13} at alkaline pH, less Al_{13} reacts with the kaolin particles by charge neutralization, which leads to the insignificant signal at 63 ppm. On the opposite, the signal at 63 ppm is detected when the dosage was increased, which could be attributed to the aggregation of the Al_{13}. Since the central AlO_4 is almost unreactive when the aggregation of Al_{13} occurs (Phillips et al., 2000), the 63 ppm signal remains intensive even though the aggregated Al_{13} is formed. Although previous studies have proved that the signal at around 62 ppm is still obtained from solid-state ^{27}Al NMR experiments of Al precipitates formed at high [OH]/[Al] ratio (Bottero et al., 1980, 1987; Furrer et al., 2002), the conditions of preparation such as concentration of total Al and [OH]/[Al] ratio could significantly affect the characteristics of Al species, including noncrystalline and crystalline Al species. At different conditions, the noncrystalline and crystalline Al species may show the same chemical properties, but differ in particle size and reactive surface. The result of solid-state ^{27}Al NMR suggests that Al_{13} is likely the predominant species to interact with kaolin particles for PACl-Al_{13} coagulation at high alkaline pH.

3.3. *Aggregates growth kinetics induced by Al_{13} aggregates*

The coagulation mechanisms significantly affect the kinetics of particle aggregation and dominate the size and structure of aggregates. Fig. 5 shows the growth profile of the aggregates coagulated by PACl-Al_{13} at pH 10, and the aggregate size is indicated by the median equivalent diameter (d_{50}). The d_{50} of the PACl-Al_{13} aggregates increases with increasing dosage and ranges from 200 μm to 250 μm with the dosage used in this work. However, the d_{50} of the aggregates formed at high dosage (8 mg/L) slowly decreases with the flocculation time. By contrast, the steady-state size of the aggregate was gradually achieved when the dosage was less than 8 mg/L. As the largest flocs are formed, the number of primary particles decreases to a minimum before the coagulation reaches the steady-state, which results in the significant decrease in the collision rate and the increase in the breakage rate. As a result,

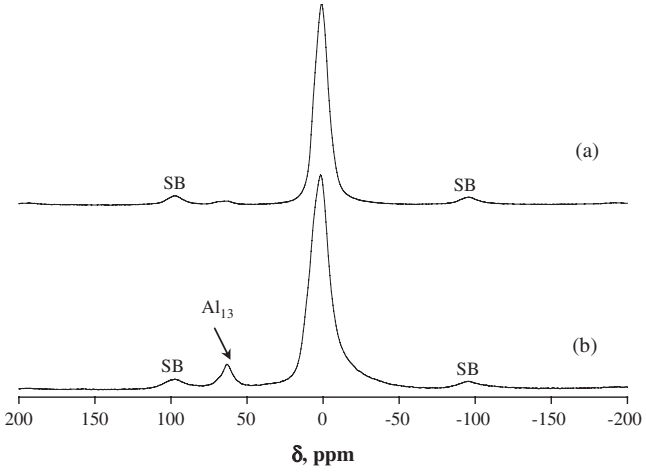

Fig. 4 – Solid-state ^{27}Al NMR spectra of the freeze-drying aggregates of PACl-Al_{13} coagulation at various dosages: (a) 1 mg/L (b) 8 mg/L.

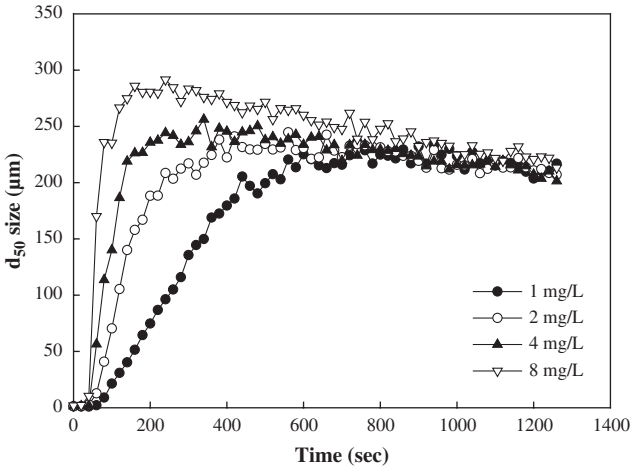

Fig. 5 – The aggregation kinetics during PACl-Al_{13} coagulation at pH 10 under various dosages.

the aggregates formed by PACl-Al_{13} at the dosage of 8 mg/L break up because larger aggregates are easily broken by eddies erosion or fragmentation (Biggs and Lant, 2000; Parker et al., 1972). The results illustrate that the growth of the flocs can be improved with higher dosage of PACl-Al_{13} during coagulation. Thus, different structures of the flocs are likely to be formed at various dosages for PACl-Al_{13} coagulation.

3.4. *Structures of PACl-Al_{13} flocs*

It has been acknowledged that the coagulation mechanisms affect the characteristics of flocs or aggregates such as fractal dimension (D_f) and morphology. The mean size and D_f of the flocs after the addition of PACl-Al_{13} under various dosages are presented in Fig. 6. The mean size of PACl-Al_{13} flocs slowly increases with increasing dosage, while the D_f of the PACl-Al_{13} flocs decreases with increasing dosage from 2.18 to 2.03. In theory, fractal dimensions do not change as a function of floc size. However, the virtual relationship between fractal dimensions and floc size tremendously hinges on the mode of particle coagulation at various conditions (Chakraborti et al., 2000; Jiang and Logan, 1996). Furthermore, the variation of the fractal dimension of kaolin flocs with the change in slow mixing time reflects the regimes of coagulation kinetics (Berka and Rice, 2005).

Table 2 shows the variation of D_f during PACl-Al_{13} coagulation at low and high dosages. At low dosage, the D_f increases slightly with slow mixing time, while the almost invariable D_f ranging from 2.04 to 2.05 at high dosage where the zero ZP is found, which is usually assigned to diffusion-limited aggregation (DLA) that rules the particle aggregation as a result of charge neutralization (Elimelech et al., 1995). However, previous studies have suggested that the invariable D_f value of flocs represents DLA with no reconstruction caused by interparticle bridging of polymer (Biggs et al., 2000; Yu et al., 2006). For PACl-Al_{13} coagulation at low dosage, the destabilization occurs (see Fig. 3), and the ZP is extremely negative and the D_f of flocs is higher than that at high dosage where the ZP is zero. In this case, if the charge neutralization dominates the coagulation at high PACl-Al_{13} dosage, the flocs formed by this way should be more compact. However, the opposite results are observed in our experiments. The results suggest that particle coagulation relies on electrostatic patch at low PACl-Al_{13} dosage and larger Al_{13} aggregates formed at high dosage can promote particle aggregation by interparticle bridging rather than charge neutralization, even though the ZP of destabilized particles are almost zero.

Table 2 – Fractal dimension of PACl-Al_{13} flocs during coagulation

Coagulants	Time (min)	Fractal dimension (D_f)	
		1 mg/L	8 mg/L
PACl-Al_{13}	10	2.14 ± 0.01	2.04 ± 0.01
	15	2.15 ± 0.01	2.04 ± 0.01
	20	2.19 ± 0.01	2.05 ± 0.01

To further verify the coagulation behavior of the Al_{13} aggregates, the WSEM was used to observe the morphology of PACl-Al_{13} flocs. The WSEM images of PACl-Al_{13} flocs at low and high dosages are shown in Fig. 7. There are marked differences between flocs formed by PACl-Al_{13} coagulation at low and high dosages. The flocs formed at low dosage are more compact and smaller, while the flocs formed at high

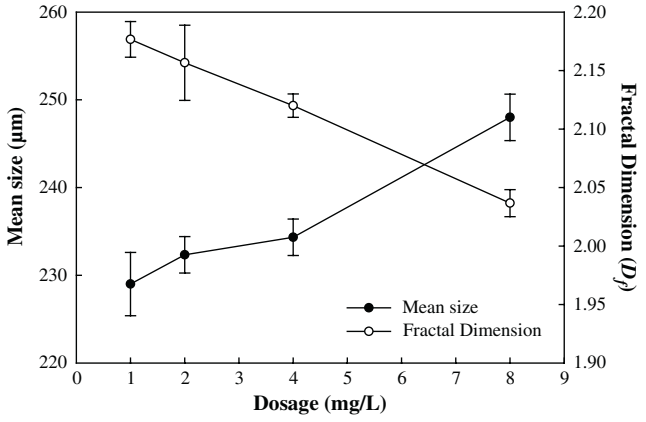

Fig. 6 – The mean size and fractal dimension of the aggregates coagulated with PACl-Al_{13} at pH 10 under various dosages.

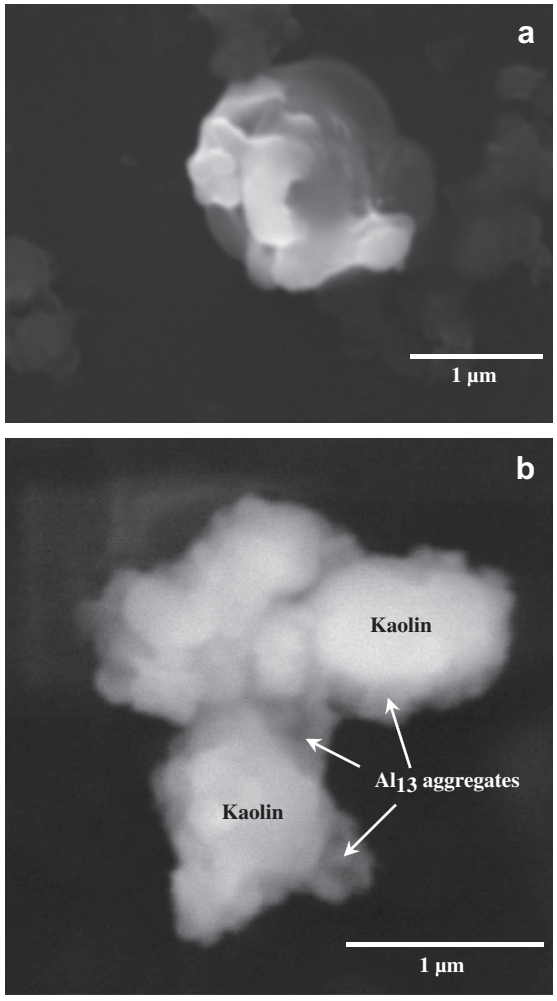

Fig. 7 – The wet SEM images of aggregates coagulated by PACl-Al_{13} at various dosages: (a) 1 mg/L and (b) 8 mg/L.

dosage have a looser structure and are larger. As shown in Fig. 7 (b), at high dosage, many Al_{13} aggregates adsorbed on the surface of the kaolin particles extend to attach other particles in the interior of PACl-Al_{13} flocs, which leads to looser structure of the flocs. The results of WSEM images conform to the observation from SASLS.

3.5. *In-situ observation on the morphology of Al_{13} aggregates*

Al_{13} molecule of various PACl coagulants has been observed by Hu et al. (2005). TM-AFM was used to observe the morphology of Al_{13} adsorbed onto the mica in air. The Al_{13} molecule, however, will condense at such condition. In this study, in-situ observation of the morphology of Al_{13} aggregates was performed by liquid TM-AFM to provide more evidences for the role of Al_{13} aggregates in the PACl-Al_{13} coagulation. The morphology of Al_{13} aggregates generated during PACl-Al_{13} coagulation at high dosage (8 mg/L) without kaolin particles in reactor was observed by TM-AFM, as shown in Fig. 8. At a high dosage, as seen in Fig. 8 (a), a few linear Al_{13} aggregates are composed of a chain of small-coiled Al_{13}. The various coiled Al_{13} aggregates are also observed in Fig. 8 (b). These single coiled Al_{13} aggregates are 300–400 nm, which are similar to the results of size measurement, as shown in Fig. 9. Moreover, they are 2–3 nm in vertical height. Although study has reported that the condensation of the nanoclusters into an X-ray amorphous gel that eventually forms bayerite with time (Bradley et al., 1993), the Al_{13} aggregates formed in our experiments should not further transform into $Al(OH)_3$ precipitates in such a short period of coagulation. The most of the Al nanoparticles are Al_{13} aggregates, not amorphous $Al(OH)_3$ precipitates. Also, the surfaces of these Al_{13} aggregates are softer as well as smoother than amorphous $Al(OH)_3$ precipitates, and they have coiled contour as well as a flat configuration of 2–3 nm. Thus, the Al_{13} aggregates formed in this study should not be $Al(OH)_3$ precipitates.

On the other hand, many studies have suggested the formation of Al_{13} aggregates is through the rearrangement of structure with aging (Bertsch et al., 1986a; Kloprogge et al., 1992). However, several researchers have advocated that the deprotonation of Al_{13} is the most possible reason for the self-assembling of Al_{13} (Letterman and Asolekar, 1990; Furrer et al., 1992). In this study, because the reaction time of coagulation is short, the exterior bound water ligands of a single Al_{13} could deprotonate as pH rises, and the exposed surface OH group of the Al_{13} has weaker charge when the dosage is increased at alkaline pH. This leads to the aggregation of defected Al_{13} with high affinity for cation in a coiled structure, as proved in Fig. 9. Different fractal dimensions imply that Al_{13} in the solution are random self-assembling in different shapes and adsorb on to the surface of the mica. As long as the efficient collision among coiled Al_{13} aggregates formed at sufficient PACl-Al_{13} dosage is achieved, these restructured Al_{13} can easily and quickly be aggregated by van der Waals attractive forces. The results echo that the higher D_f of Al_{13} aggregates is attributed to the denser Al_{13} within the Al_{13} aggregates (Axeols et al., 1986). The linear Al_{13} aggregates formed in the alkaline condition has also been proposed by Bottero et al. (1987) in the

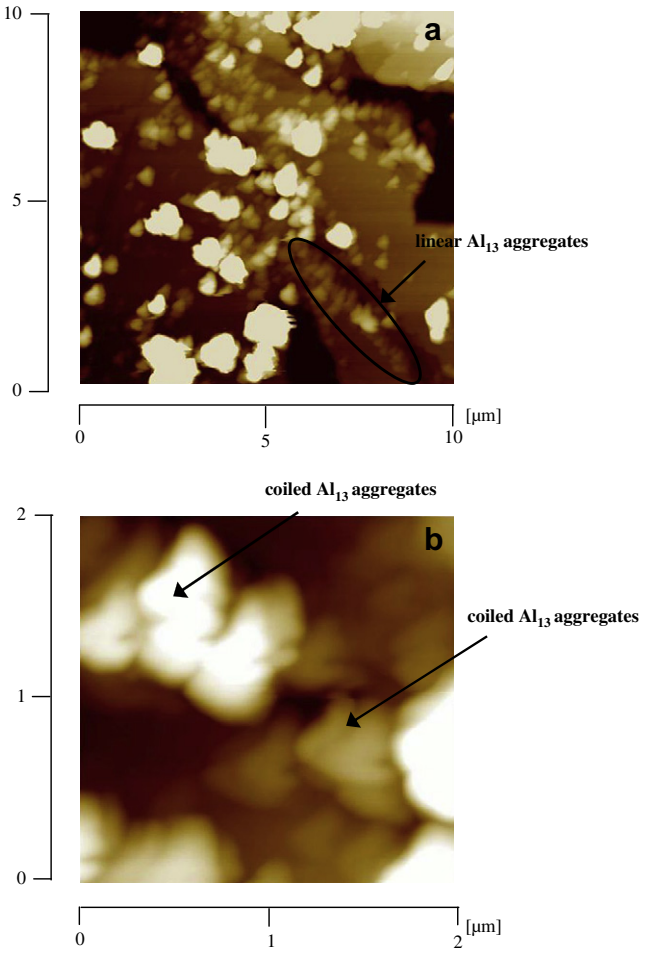

Fig. 8 – TM-AFM topographic image of the Al_{13} adsorbed on the mica at pH 10 in liquid system.

model calculation on the configuration of aggregated Al_{13} with small angle X-ray scattering (SAXS). Our study is the first work that obtains the linear image of aggregated Al_{13} in liquid system.

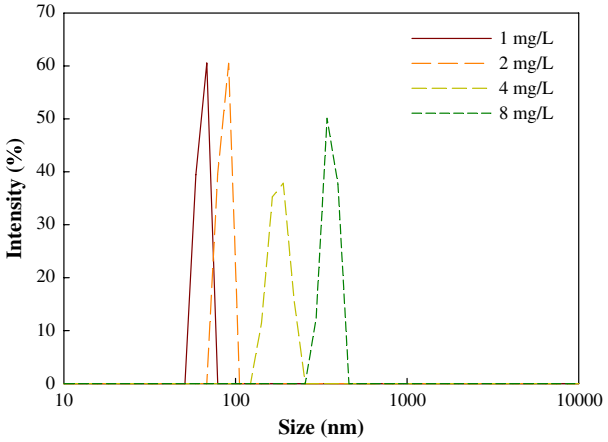

Fig. 9 – Size distributions of Al_{13} in PACl-Al_{13} coagulation at various dosages without kaolin particles.

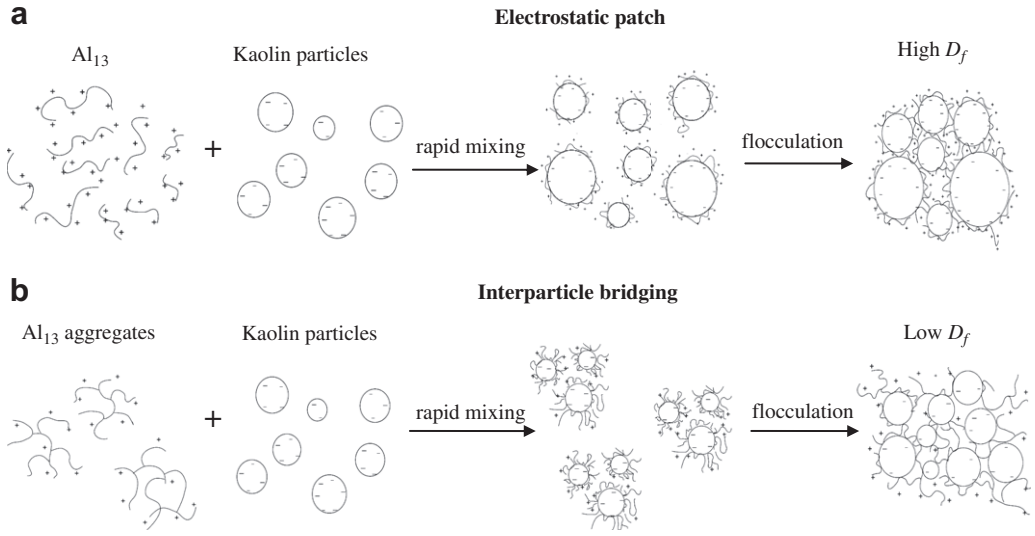

Fig. 10 – Schematic representation of the PACl-Al_{13} coagulation mechanism induced by Al_{13} and Al_{13} aggregates. (a) electrostatic patch (b) interparticle bridging.

3.6. *Predominant coagulation mechanisms of Al_{13} and Al_{13} aggregates*

The coagulation mechanisms of cationic polymers in coagulation of colloidal particles are well-known, including charge neutralization, interparticle bridging and electrostatic patch (Gregory, 1973). These mechanisms can happen concurrently and are frequently competing with each other. The coagulant dosage also has influences on the conformation of polymer and consequently the adsorption on the surface of particles, which causes different mechanisms of coagulation (Zhou and Franks, 2006). As a result, the Al_{13} conformation on the surface of particles will change under different PACl-Al_{13} dosages, inducing different coagulation mechanisms.

For PACl-Al_{13} coagulation at high alkaline, since increasing the dosage accompanies the formation of Al_{13} aggregates, the mechanisms between the reaction of Al_{13} aggregates and particles will change correspondingly. The schematics of predominant mechanisms of PACl-Al_{13} coagulation at low and high dosages are presented in Fig. 10 (a) and (b), respectively. At low dosage, because of the repulsion between weakly positively charged Al_{13} molecules, the larger Al_{13} aggregates cannot be easily generated via Al_{13} self-assembling. As a result, the weakly positively charged Al_{13} can only adsorb onto the surface as flattened configuration and then perform the particle coagulation by electrostatic patch, which contributes to the high D_f of PACl-Al_{13} flocs. At high dosage, linear Al_{13} aggregates with a given dimension or other dimensional Al_{13} aggregates can rapidly form via the collisions of coiled Al_{13} aggregates and then adsorb onto kaolin particle surface as extended configuration when the surfaces of particles are clouded. Therefore, the extended Al_{13} aggregates adsorbed on particle surface can assemble particles by interparticle bridging, which results in the low D_f of PACl-Al_{13} flocs.

4. Conclusions

For PACl-Al_{13} coagulation, electrostatic patch is responsible for particle destabilization at high alkaline pH (pH 10) when the low dosage is applied, which results in high fractal dimension (D_f) of aggregates. Interparticle bridging becomes the major mechanism when the sufficient high dosage is applied due to the formation of Al_{13} aggregates, which leads to flocs with low D_f, even though the ZP of destabilized particles is zero at such condition. The images of flocs observed via WSEM are in accordance with the results of fractal dimension analysis. During PACl-Al_{13} coagulation, the flocs formed by interparticle bridging are more easily broken during coagulation processes by shear stress. In addition, the size of Al_{13} aggregates increases with PACl-Al_{13} dosage. Some larger linear Al_{13} aggregates compose of a chain of coiled Al_{13} as a result of weakly charged Al_{13} self-assembling. Several coiled Al_{13} aggregates with different dimensions are also observed at such conditions. This is the foremost finding in the observation of Al_{13} aggregates under liquid environment. For PACl coagulation in high alkaline water, the formation of large linear or coiled Al_{13} aggregates can efficiently promote particle coagulation by interparticle bridging.

Acknowledgement

This research was supported by the grant of National Science Council, ROC (NSC 97-2221-E-009-069-MY3).

REFERENCES

Akitt, J.W., Farthing, A., 1981. Aluminium-27 nuclear magnetic resonance studies of the hydrolysis of aluminium (III). Part V.

Slow hydrolysis using aluminum metal. J. Chem. Soc. Dalton Trans., 1624–1626.
Arita, T., Kanda, Y., Higashitani, K., 2004. In situ observation of single polymers adsorbed onto mica surfaces in water. J. Colloid Interface Sci. 273, 102–105.
Axeols, M.A.V., Tchoubar, D., Jullien, R., 1986. X-ray scattering functions of fractal structures: comparison between simulations and experiments. J. Phys. 47 (10), 1843–1847.
Berka, M., Rice, J.A., 2005. Relation between aggregation kinetics and the structure of kaolinite aggregates. Langmuir 21, 1223–1229.
Bertsch, P.M., Layton, W.J., Barnhisel, R.I., 1986a. Speciation of hydroxyaluminum solutions by wet chemical and aluminum. Soil Sci. Soc. Am. J. 50, 1449–1454.
Bertsch, P.M., Tohmas, G.W., Barnhisel, R.I., 1986b. Characterization of hydroxy-aluminum solutions by aluminum-27 nuclear magnetic resonance spectroscopy. Soil Sci. Soc. Am. J. 50, 825–830.
Biggs, C.A., Lant, P.A., 2000. Activated sludge flocculation: on-line determination of floc size and the effect of shear. Water Res. 34, 2542–2550.
Biggs, S., Habgood, M., Jameson, G., Yan, Y.D., 2000. Aggregate structures formed via a bridging flocculation mechanism. Chem. Eng. J. 80, 13–22.
Bottero, J.Y., Axelos, M., Tchoubar, D., Cases, J.M., Fripiat, J.J., Fiessinger, F., 1987. Mechanism of formation of aluminum trihydroxide form Keggin Al_{13} polymers. J. Colloid Interface Sci. 117, 47–57.
Bottero, J.Y., Cases, J.M., Fiessinger, F., Poirier, J.E., 1980. Studies of hydrolyzed aluminum chloride solutions. I. Nature of aluminum species and composition of aqueous solutions. J. Phys. Chem. 84, 2933–2939.
Bradley, S.M., Kydd, R.A., Howe, R.F., 1993. The structure of Al-gels formed through base hydrolysis of Al^{3+} aqueous solutions. J. Colloid Interface Sci. 159, 405–412.
Chakraborti, R.K., Atkinson, J.F., Van Benschoten, J.E., 2000. Characterization of alum floc by image analysis. Environ. Sci. Technol. 34, 3969–3976.
Chen, Z.Y., Fan, B., Peng, X.J., Zhang, Z.G., Fan, J.H., Luan, Z.K., 2006. Evaluation of Al_{30} polynuclear species in polyaluminum solutions as coagulant for water treatment. Chemosphere 64, 912–918.
Chin, C.J., Yiacoumi, S., Tsouris, C., 2002. Influence of metal ion sorption on colloidal surface forces measured by atomic force microscopy. Environ. Sci. Technol. 36, 343–348.
Dentel, S.K., 1988. Application of the precipitation-charge neutralization model of coagulation. Environ. Sci. Technol. 22, 825–832.
Dubbin, W.E., Sposito, G., 2005. Copper-glyphosate sorption to microcrystalline gibbsite in the presence of soluble Keggin Al-13 polymer. Environ. Sci. Technol. 39, 2509–2514.
Elimelech, M., Gregory, J., Jia, X., Williams, R.A., 1995. Particle Deposition and Aggregation: Measurement, Modeling and Simulation. Butterworth-Heinemann Ltd., Oxford.
Furrer, G., Gfeller, M., Wehrli, B., 1999. On the chemistry of the Keggin Al-13 polymer: kinetics of proton-promoted decomposition. Geochim. Cosmochim. Acta 63, 3069–3076.
Furrer, G., Ludwig, C., Schindler, P.W., 1992. On the chemistry of the Keggin Al_{13} polymer. 1. Acid-base properties. J. Colloid Interface Sci. 149, 56–67.
Furrer, G., Phillips, B., Ulrich, K.U., Pöthig, R., Casey, W.H., 2002. The origin of aluminum flocs in polluted streams. Science 297, 2245–2247.
Gao, B.Y., Chu, Y.B., Yue, Q.Y., Wang, B.J., Wang, S.G., 2005. Characterization and coagulation of a polyaluminum chloride (PAC) coagulant with high Al_{13} content. J. Environ. Manage. 76, 143–147.
Gregory, J., 1973. Rates of flocculation of latex particles by cationic polymers. J. Colloid Interface Sci. 42, 448–456.
Guan, J., Waite, T.D., Amal, R., 1998. Rapid structure characterization of bacterial aggregates. Environ. Sci. Technol. 32, 3735–3742.
Hu, C.Z., Liu, H.J., Qu, J.H., 2005. Preparation and characterization of polyaluminum chloride containing high content of Al_{13} and active chlorine. Colloids Surface A 260, 109–117.
Hu, C.Z., Liu, H.J., Qu, J.H., Wang, D.S., Ru, J., 2006. Coagulation behavior of aluminum salts in eutrophic water: significance of Al_{13} species and pH control. Environ. Sci. Technol. 40, 325–331.
Ikai, A., 1996. STM and AFM of bio/organic molecules and structures. Surf. Sci. Rep. 26 (8), 261–332.
Jiang, Q., Logan, B.E., 1996. Fractal dimensions of aggregates from shear devices. J. Am. Water Works Assoc. 88 (2), 100–113.
Johansson, G., 1960. On the crystal structures of some basic aluminum salts. Acta Chem. Scand. 14, 771–773.
Katz, A., Bentur, A., Kovler, K., 2007. A novel system for in-situ observations of early hydration reactions in wet conditions in conventional SEM. Cement Concr. Res. 37, 32–37.
Kazpard, V., Lartiges, B.S., Frochot, C., d'Espinose de la Caillerie, J. B., Viriot, M.L., Portal, J.M., Görner, T., Bersillon, J.L., 2006. Fate of coagulant species and conformational effects during the aggregation of a model of a humic substance with Al_{13} polycations. Water Res. 40, 1965–1974.
Kloprogge, J.T., Seykens, D., Jansen, J.B.H., Geus, J.W., 1992. A ^{27}Al nuclear magnetic resonance study. J. Non-Cryst. Solids 142, 94–102.
Letterman, R.D., Vanderbrook, S.G., Sricharoenchaikit, P., 1982. Electrophoretic mobility measurements in coagulation with aluminum salts. J. AWWA 74, 44–51.
Letterman, R.D., Asolekar, S.R.A., 1990. Surface ionization of polynuclear species in Al(III) hydrolysis-1. Titration results. Water Res. 24, 931–939.
Li, D.H., Ganczarczyk, J.J., 1989. Fractal geometry of particle aggregates generated in water and wastewater treatment processes. Environ. Sci. Technol. 23, 1385–1389.
Lin, J.L., Huang, C.P., Pan, J.R., Wang, D.S., 2008. Effect of Al(III) speciation on coagulation of highly turbid water. Chemosphere 72, 189–196.
Lin, M.Y., Lindsay, H.M., Weita, D.A., Ball, R.C., Klein, R., Meakin, P., 1989. Universality in colloid aggregation. Nature 339, 360–362.
Liu, G.G., Qu, J.H., Tang, H.G., 1999. The electrochemical production of highly effective polyaluminum chloride. Water Res. 33 (3), 807–813.
Mandelbrot, B.B., 1983. The Fractal Geometry of Nature. W.H. Freeman and Co., New York.
Nalaskowski, J., Veeramasuneni, S., Hupka, J., Miller, J.D., 1999. AFM measurements of hydrophobic forces between a polyethylene sphere and silanated silica plates – the significance of surface roughness. J. Adhes. Sci. Technol. 13, 1519–1533.
Parker, D.S., Kaufman, W.J., Jenkins, D., 1972. Floc breakup in turbulent flocculation processes. J. Sanit. Eng. Div.: Proc. Am. Soc. Civ. Eng. SA1, 79–99.
Phillips, B.L., Casey, W.H., Karlsson, M., 2000. Bonding and reactivity at oxide mineral surfaces from model aqueous complexes. Nature 404, 379–382.
Rakotonarivo, E., Bottero, J.Y., Thomas, F., Poirier, J.E., Cases, J.M., 1988. Electrochemical modelling of freshly precipitated aluminum hydroxide-electrolyte interface. Colloid Surface 33, 191–207.
Sanz, J., Serratosa, J.M., 1984. ^{29}Si and ^{27}Al high-resolution MAS-NMR spectra of phyllosilicates. J. Am. Chem. Soc. 106, 4790–4793.

Shi, B.Y., Li, G.H., Wang, D.S., Tang, H.X., 2007. Separation of Al_{13} from polyaluminum chloride by sulfate precipitation and nitrate metathesis. Sep. Purif. Technol. 54, 88–95.

Sposito, G.E., 1996. The Environmental Chemistry of Aluminium, second ed. CRC Press, Inc.

Violante, A., Huang, P.M., 1985. Influence of inorganic and organic-ligands on the formation of aluminum hydroxides and oxyhydroxides. Clays Clay Miner. 33, 181–191.

Waite, T.D., Cleaver, J.K., Beattie, J.K., 2001. Aggregation kinetics and fractal structure of gamma-alumina assemblages. J. Colloid Interface Sci. 241, 333–339.

Wang, D.S., Sun, W., Xu, Y., Tang, H.X., Gregory, J., 2004. Speciation stability of inorganic polymer flocculant-PACl. Colloid Surface A 243, 1–10.

Wang, W.Z., Hsu, P.H., 1994. The nature of polynuclear OH–Al complexes in laboratory-hydrolyzed and commercial hydroxyaluminum solutions. Clays Clay Miner. 42, 356–368.

Wu, R.M., Lee, D.J., Waite, T.D., Guan, J., 2002. Multilevel structure of sludge flocs. J. Colloid Interface Sci. 252, 383–392.

Wu, X.H., Ge, X.P., Wang, D.S., Tang, H.X., 2007. Distinct coagulation mechanism and model between alum and high Al13-PACl. Colloid Surface A 305, 89–96.

Yan, M.Q., Wang, D.S., Qu, J.H., He, W.J., Chow, C.W.K., 2007. Relative importance of hydrolyzed Al(III) species (Ala, Alb, and Alc) during coagulation with polyaluminum chloride: a case study with the typical micro-polluted source waters. J. Colloid Interface Sci. 316, 482–489.

Ye, C.Q., Wang, D.S., Shi, B.Y., Yu, J.F., Qu, J.H., Edwards, M., Tang, H.X., 2007. Alkalinity effect of coagulation with polyaluminum chlorides: role of electrostatic patch. Colloid Surface A 294, 163–173.

Yu, J.F., Wang, D.S., Ge, X.P., Yan, M.Q., Yang, M., 2006. Flocculation of kaolin particles by two typical polyelectrolytes: a comparative study on the kinetic and flocs structures. Colloid Surface A 290, 288–294.

Zhou, Y., Franks, G.V., 2006. Flocculation mechanism induced by cationic polymers investigated by light scattering. Langmuir 22, 6775–6786.